Numerical Investigation of Thermal Performance of a Combined Heat Sink with Various Microchannel Shapes

A. Q. Lawal, O. O. Adewumi*, O. T. Olakoyejo

Department of Mechanical Engineering, University of Lagos, Akoka, Nigeria.

ABSTRACT: The influence of channel shape on a combined heat sink of three different channel forms is investigated numerically in this work. The channel shapes considered were the trapezoidal, inverse trapezoidal and hexagonal microchannel shapes. The goal of this study was to compare and identify the combined microchannel shape that performed best under conditions of high uniform heat flux. The thermal performance of the combined heat sink was assessed using two criteria: lowest maximum temperature and lowest temperature elevation on the bottom of the combined heat sink where heat is applied. The uniform heat flux applied to the bottom of the combined heat sink was elevated from $100\ W/cm^2$ to$1000\ W/cm^2$. For the maximum heat flux of $1000\ W/cm^2$and lowest pressure drop of 10kPa considered, in terms of temperature elevation on the bottom of the heat sink where heat is applied, the trapezoidal combined microchannel heat sink outperformed other channel shapes. When the minimized overall maximum temperature is considered, the hexagonal combined microchannel heat sink was the best combined heat sink.

KEYWORDS: Thermal performance; Uniform heat flux; Temperature; Combined heat sink; Microchannel shape

[Received Mar. 10, 2022; Revised May 18, 2022; Accepted May 18, 2022] Print ISSN: 0189-9546 | Online ISSN: 2437-2110

I. INTRODUCTION

Increasing energy demands, the need for improved energy efficiency, space constraints for system packaging, and increased flexibility and machine handling ease have all provided challenges for producing high performance heat exchangers. Innovative microchannel heat exchangers, among other approaches, prove to be the most viable way to address these thermal control problems. High-performance heat sinks are needed to ensure the integrity and durability of the processor of such systems. As a result, different heat sinks have been developed for cooling to ensure microelectronics operate within allowable temperature limit. Several research on the utilization and optimization of microchannel heat sinks have been performed in the previous decade (Wei and Joshi, 2003). Tuckerman and Pease (1981) first carried out research on microchannel heat sinks and projected that single-phase forced convective cooling in microchannels could theoretically extract heat at a rate of 1,000 W/m^2.

To minimize peak temperature, Adewumi *et al* (2013) applied constructal theory to geometrically optimize a combined microchannel heat sink for both constant and variable axial lengths. Their numerical study showed that combined rectangular microchannel with micro pin fins exhibits better thermal performance than microchannels not having pin fins, according to their research. Some other analytical, experimental and numerical studies that considered other microchannel shapes are Chen *et al* (2009), Meyer *et al* (2012), Olakoyejo *et al* (2012), Salimpour *et al* (2013), Khan and Kim (2013), Garg *et al* (2014), Teja *et al* (2014), Glazar *et al* (2015), Khan *et al* (2016), Magnini and Matar (2020) and Jagadale *et al* (2020) to mention a few. All these works did not investigate the thermal performance of a combination of these different microchannel shapes with micro pin-fins.

Research were also carried out on the performance of different shapes of pin-fin heat sinks. Olakoyejo and Meyer (2014) applied constructal theory to numerically optimize square pin fins to minimize thermal resistance and reduce peak temperature, with the heat sink subjected to a constant temperature. The geometric parameters of the pin fins were found to be insensitive to their configuration. Other thermal performance studies on pin-fin heat sinks were carried out by Khan *et al* (2006), Abdel-Rehim (2008), Izci *et al* (2015), Bello-Ochende (2015), Hasan and Tbena (2018), Roy and Kundu (2018), Jadhav *et al* (2018), Yadav and Pandeya (2018) to mention a few.

There were also investigations on the comparison between the performance microchannels and micro pin-fins. Hasan and Muter (2019) analyzed the hydraulic and thermal performance of rectangular microchannel heat sinks to rectangular, triangular micro pin fins using various coolants. They experimented with three distinct pure fluids (water, oil, and ethylene glycol). For all shapes tested, circular pin fins performed better in terms of thermal performance.

All literature reviewed showed that rectangular, semicircular, triangular, and trapezoidal cross-sections are the most commonly employed shapes of microchannel heat sinks.

The goal of this study is to numerically assess the thermal performance of various microchannel shapes when combined with circular-shaped micro pin-fins. The results will be

*Corresponding author: oadewunmi@unilag.edu.ng *doi:* http://dx.doi.org/10.4314/njtd.v19i2.9

compared with those obtained for a combined heat sink with rectangular microchannels presented by Adewumi *et al* (2013). The microchannel shape which performs best in reducing the maximum temperature and temperature variation along the bottom of the combined heat sink is chosen as the best shape in this study. For microelectronic cooling applications, the combined heat sink with the lowest maximum temperature and least bottom wall temperature variation will be recommended.

II. MODEL DESCRIPTION, GOVERNING EQUATIONS AND BOUNDARY CONDITIONS

The simulation domain for the combined heat sink with different microchannel shapes and circular micro pin-fin inserts of elemental volume, *V*, is shown in Figure 1.

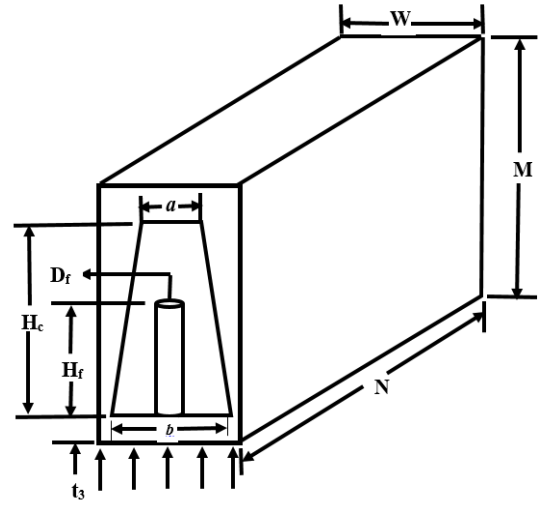

(a)

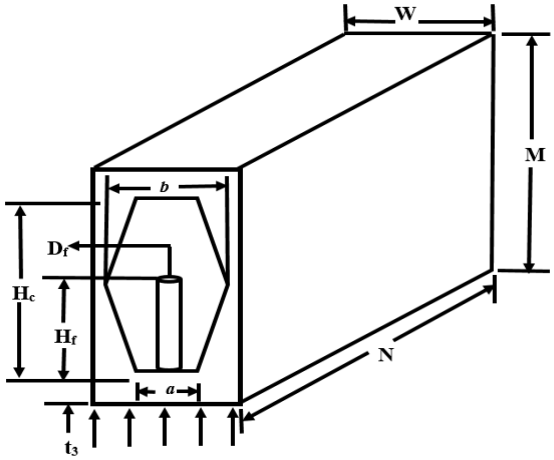

(b)

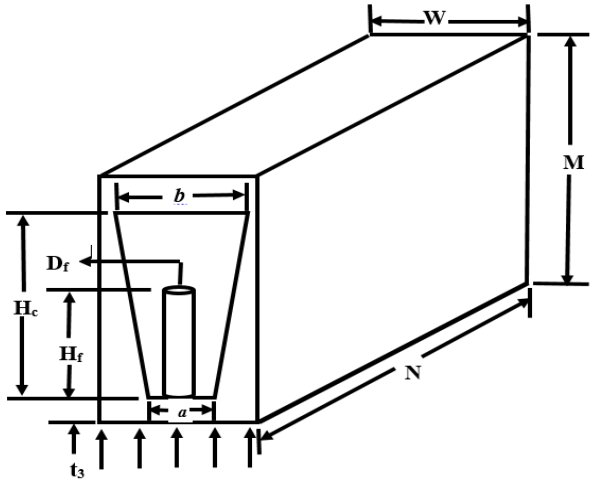

(c)

Figure 1: Computational domain of combined heat sink with (a) trapezoidal- (b) inverse trapezoidal- (c) hexagonal-shaped microchannels

By numerically solving the conservation of mass, momentum, and energy equations, the temperature variation within the combined heat sinks considered in this work was determined. Fluid flow and heat transfer analysis are controlled by the governing Eqns. (1) to (7):

$$\nabla . \vec{v} = 0 \quad (1)$$

$$\rho(\vec{v}.\nabla\vec{v}) = -\Delta P + \mu\nabla^2\vec{v} \quad (2)$$

$$\rho_f C_{pf}(\vec{v}.\nabla T) = k_f\nabla^2 T \quad (3)$$

The energy equation for the solid regions can be written as:

$$k_s\nabla^2 T = 0 \quad (4)$$

The heat flux between the fluid and solid interface is connected and its continuity between the solid and liquid surfaces is given as Eqn. (5):

$$k_s \frac{\partial T}{\partial n}\Big|_{wall} = k_f \frac{\partial T}{\partial n}\Big|_{wall} \quad (5)$$

There is no sliding and penetration on the wall surface and the other boundary conditions are: At inlet, $P = P_{in},\ v = w = 0$; at outlet, $P_{out} = P_{atm}$ and $T = T_{in}$; $\frac{\partial T}{\partial x} = 0$ specifies the symmetry boundary conditions on both sides of the computing domain. The bottom wall is exposed to a steady uniform thermal flux $q'' = k_s \frac{\partial T}{\partial y}$. The maximum global thermal conductance is the performance metric, which in dimensionless form, is

$$C_{max} = \frac{q''N}{k_f \Delta T} \quad (6)$$

The temperature rise in the domain is defined by:

$$\Delta T = T_{max} - T_{min} \quad (7)$$

III. NUMERICAL SOLUTION PROCEDURE

A three-dimensional computational fluid dynamics (CFD) tool, ANSYS Fluent, that makes use of the finite volume approach, was applied to solve the boundary conditions, as well as the continuity, momentum, and energy Eqns (1) to (5) numerically. A tetrahedron element was used to finely mesh the computational domain. The combined convection and

diffusion elements of the momentum and energy equations were discretized using a second-order upwind approach.

When the standardised residuals of the continuity and momentum equations falls below 10^{-5} and that of the energy equation falls below 10^{-7}, the solution is expected to converge. The convergence condition for the peak temperature as the quantity monitored is:

$$\gamma = \left|\frac{\Delta T_i - \Delta T_{i-1}}{\Delta T_i}\right| \leq 0.01 \quad (8)$$

where *i* is the mesh iteration index and the mesh, more refined as *i* increases . The *i* - 1 mesh is selected when the convergence criterion in Eqn (8) is satisfied.

The dimensions of the combined heat sink with trapezoidal-, inverse trapezoidal- and hexagonal-shaped microchannels used for the grid refinement test are shown in Table 1. Grid refinement test was carried out on the combined heat sinks at a pressure drop of ΔP = 30 kPa. The results for the grid refinement for the combined heat sink with trapezoidal-, inverse trapezoidal-, and hexagonal-shaped microchannels are shown in Tables 2, 3 and 4 respectively. For the numerical simulations, 1,043,448 cells were used for the trapezoidal combined heat sink, 1,128,754 for the inverse trapezoidal and 1,472,697 for the hexagonal combined heat sink.

Table 1: Dimensions of the trapezoidal, inverse trapezoidal and hexagonal combined heat sink heat sink for grid refinement test.

$H_c\ (\mu m)$	$a\ (\mu m)$	$b\ (\mu m)$	$W_s\ (\mu m)$
759.83	47.84626	76.42974	100
$H_c\ (\mu m)$	$t_3 (\mu m)$	d_{f1} **to** $d_{f6}\ (\mu m)$	h_{f1} **to** $h_{f6} (\mu m)$
900	56.505	40	160

Table 2: Grid refinement test results for the trapezoidal combined heat sink.

Number of cells	ΔT (K)	γ
349631	2.204	0
524778	8.814	2.9999
784338	8.904	0.0102
1043448	8.990	0.0097
1398777	9.076	0.0095

Table 3: Grid refinement test results for the inverse trapezoidal combined heat sink.

Number of Cells	$\Delta T\ (K)$	γ
382081	8.4273	-------
576501	8.5793	0.1080
805902	8.7112	0.0154
1128754	8.7780	0.0077
1449915	8.8527	0.0085

Table 4: Grid refinement test results for the hexagonal combined heat sink.

Number of Cells	$\Delta T\ (K)$	γ
349749	5.8949	-------
530564	8.4737	0.4375
746209	8.5858	0.1322
1219008	8.7062	0.0140
1472697	8.7790	0.0084

The CFD code used in this study has been validated previously in the work by Adewumi *et al* (2013) with an analytical and numerical investigations by Khan *et al* (2006) and Bello-Ochende *et al* (2010) respectively. Piecewisell linear function of temperature was used to characterize the thermophysical characteristics of water to capture the changes in the properties of water as temperature changes within the elemental computation domain, as indicated in Eqn. (9) (ANSYS FLUENT, 2011). Natural convection and radiation are presumed to be insignificant.

$$\eta(T) = \eta_a + \frac{\eta_{a+1} - \eta_a}{T_{a+1} - T_a}(T - T_a) \quad (9)$$

where $1 \leq a \leq L$ and L are the number of segments while η is the coolant property. The temperature variation on the bottom of the combined heat sink is given by,

$$(\Delta T)_{base} = (T_{max} - T_{min})_{base} \quad (10)$$

All combined microchannels were numerically simulated at a constant volume *V* of $0.9mm^3$ with a fixed axial length *N* of $10\ mm$ The water pushed through the microchannel was at temperature 20°C at the inlet, the base of the combined heat sink was exposed to a total thermal flux ranging from $100\ W/cm^2$ to $1000\ W/cm^2$, with a pressure drop range of $10kPa \leq \Delta P \leq 60kPa$.

IV. OPTIMISATION OF DESIGN VARIABLES

The length (*N*), height (*M*) and width (*W*) of the solid are constant, as well as the volume *V*, while variation in t_1, t_2, t_3, H_c and W_c was allowed with manufacturing restrictions imposed. The entire volume of the combined heat sink is given as:

$$V = WMN = constant \quad (11)$$

Using the channel and solid substrate dimensions, the porosity ϕ (also known as the solid volume fraction) of the combined heat sink is calculated. The ratio of the solid volume to the entire volume ratio is solely determined by the heat sink's cross-sectional area, as shown in Eqn. (12).

$$\phi = \frac{V_{solid}}{V} = \frac{A_{solid}}{A} = \frac{MW - H_c W_c}{MW} \quad (12)$$

The following are the manufacturing limits for heat sinks

$$\frac{H_c}{W_c} \leq 20 \quad (13)$$

$$t_2 \leq 50\mu m \quad (14)$$

$$M - t_2 \leq 50\mu m \quad (15)$$

The manufacturing constraints in Eqns (16) and (17) are also applied to the combined heat sinks.

$$0.5 \leq \frac{H_f}{D_f} \leq 4.0 \quad (16)$$

$$s \geq 50\mu m \quad (17)$$

The volume of the cylindrical fins is constant and a total fin volume constraint is imposed on the micro pin fins.

$$V_f = V_{f1} + V_{f2} + \cdots + V_{fn} = constant \quad (18)$$

V. RESULTS AND DISCUSSION

The sub-sections below present the findings on the effect of the different microchannel shapes on the thermal conductance and temperature variation along the heated bottom of the combined heat sink.

A. Effect of Increasing Heat Flux on the Minimized Peak Temperature

Figure 2(a) shows the result of rising heat flux on the minimum peak temperature for a trapezoidal, inverse trapezoidal, and hexagonal combined microchannel heat sink with a constant volume V of 0.9 mm^3, a constant pressure drop (ΔP) of 60 kPa, and a fixed axial length N of 10 mm. Along the heated bottom of the combined heat sink, the thermal flux $q"$ was steadily increased from 100 W/cm^2 to 1000 W/cm^2. It was observed that the combined heat sink with hexagonal-shaped microchannel had the least peak temperature from 100 W/cm^2 to 1000 W/cm^2. For a pressure drop of 10kPa, the minimized peak temperature increased by approximately 79% for all combined heat sink considered in this present study when the heat flux was increased from 100 W/cm^2 to 1000W/cm^2 (90% increase).

A pressure drop increase to 60 kPa resulted in the minimized peak temperature increase of approximately 70% for all the combined heat sink when heat flux was increased from 100 W/cm^2 to 1000 W/cm^2. A pressure drop of 60 kPa gave lowest peak temperature of 26.51 °C for heat flux of 100 W/cm^2 and 88.03 °C for 1000 W/cm^2. The combined heat sink with trapezoidal-shaped microchannel had the highest peak temperature. The combined heat sink with hexagonal-shaped microchannel reduced the minimized peak temperature 4.2% when compared with the trapezoidal-shaped counterpart at 1000 W/cm^2 heat flux and pressure drop of 60kPa. This shows increased thermal conductance of which the combined heat sink with hexagonal-shaped microchannels had the best performance as shown in Figure 2(b).

B. Effect of Increasing Pressure Drop On Minimized Peak Temperature

In the previous study carried out by Adewumi *et al* (2013) where the thermal performance of the combined heat sink with rectangular-shaped microchannels was investigated, the minimized peak temperature obtained for heat flux of 100 W/cm^2, pressure drop of 10 kPa and 60 kPa was 41.38 ˚C and 28.62 ˚C respectively. In this present study, considering the same heat flux and pressure drops, the minimized peak temperature was reduced to 34.83 ˚C and 27.19 ˚C respectively for the trapezoidal-shaped configuration, 34.84˚C and 26.85˚C respectively for the inverse trapezoidal-shape, 34.51˚C and 26.5 ˚C respectively for the hexagonal-shape.

These results are presented in Figure 3(a). A comparison between the combined heat sink with rectangular-shaped microchannels for pressure drop of 10 kPa showed that the combined heat sink with trapezoidal- and inverse trapezoidal-decreased the minimized peak temperature by 15.8% while the combined heat sink with hexagonal-shaped microchannels gave a decreased minimized peak temperature of 16.6%.

For a pressure drop of 60 kPa, the combined heat sink with trapezoidal-, inverse trapezoidal- and hexagonal-shaped microchannels reduced the minimized peak temperature by 5%, 6.2% and 7.4% respectively when compared to the combined heat sink with rectangular-shaped microchannel. The hexagonal combined heat sink had the lowest peak temperature of 88.03 °C at the heated bottom wall, 88.76 °C for the inverse-trapezoidal and 91.85 °C for the trapezoidal combined heat sink when the heat flux was fixed at 1000 W/cm^{2}and pressure drop of 60 kPa as shown in Figure 3(b).

C. Temperature Variation along the Heated Base of the Solid Substrate under High Thermal Flux

Presented in this section is the numerical investigation of the temperature variation along the bottom wall of the combined heat sinks. The lowest temperature difference, $(\Delta T)_{base}$ will be used to determine the combined heat sink with the lowest temperature gradient. This is very important in ensuring that a microelectronic device does not fail as a result of steep temperature gradient giving rise to high thermal stresses in the bottom wall.

Figure 4 shows the temperature gradient along bottom wall for the combined heat sink with trapezoidal-shaped microchannel when a minimum heat flux of 100 W/cm^2 and maximum of 1000 W/cm^2 is applied. For a pressure drop of

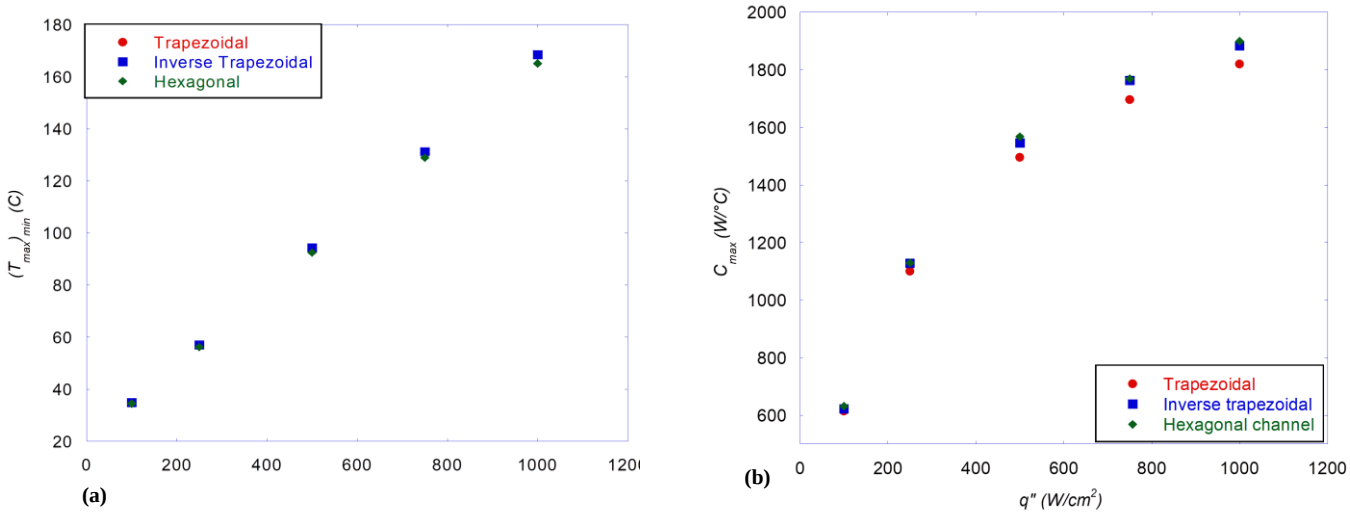

Figure 2: Effect of increasing heat flux on (a) minimized peak temperature (b) maximized thermal conductance in combined heat sink with different microchannel shapes.

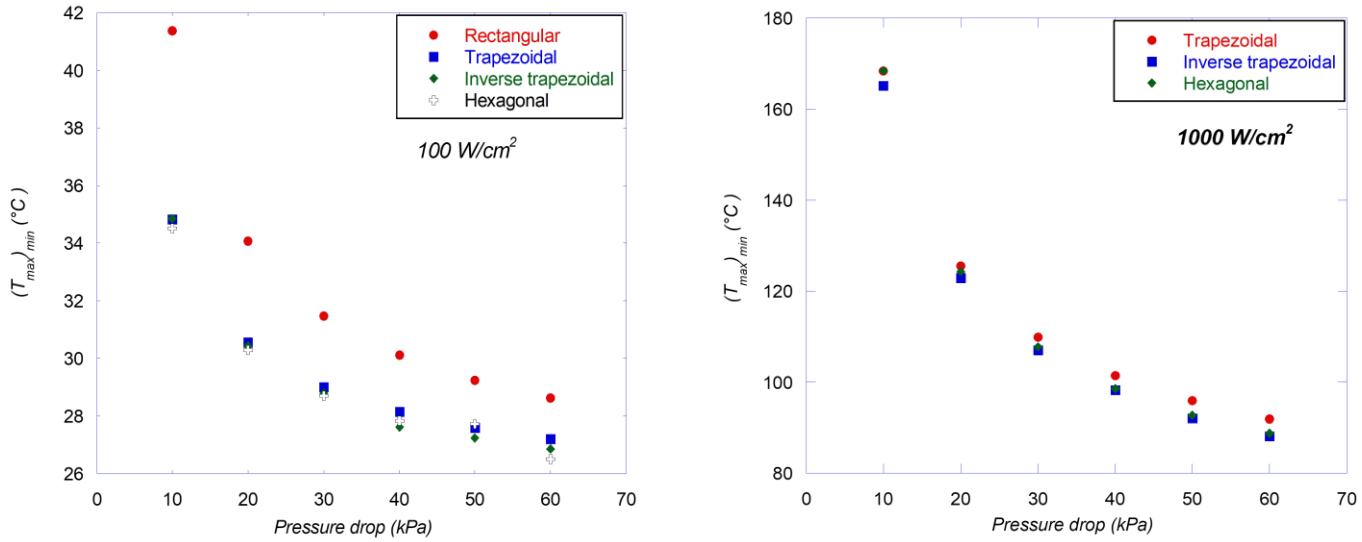

Figure 3: Minimized peak temperature in combined heat sink with different microchannel shapes at different pressure drops (a) 100 W/cm² (b) 1000 W/cm².

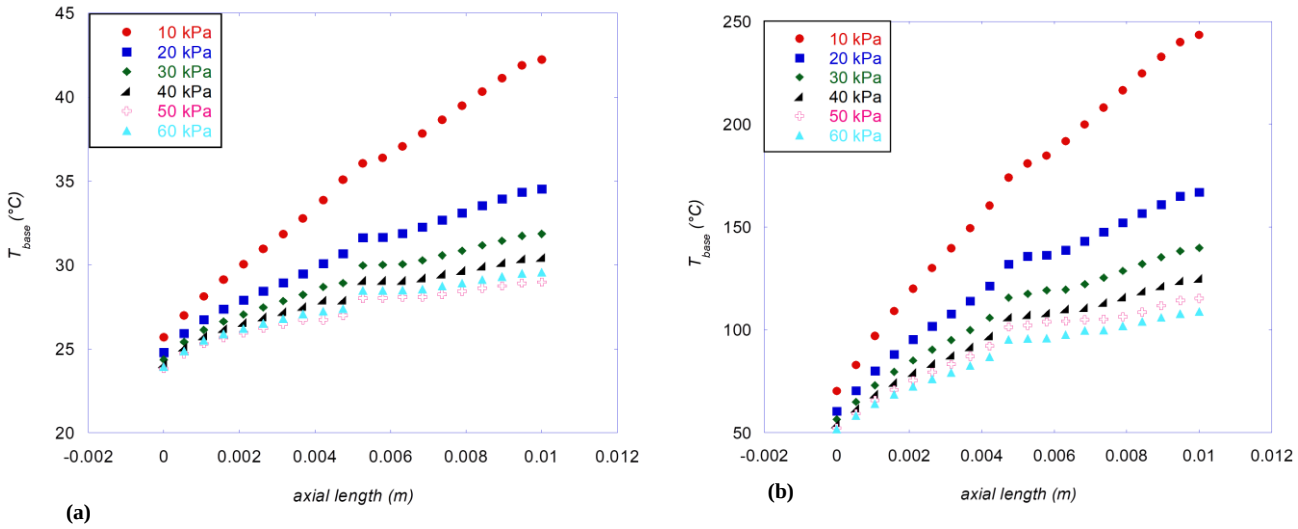

Figure 4: Temperature gradient along the bottom wall of the combined heat sink with trapezoidal-shaped microchannel (a) 100 W/cm² (b) 1000 W/cm².

10 kPa and heat flux of 100 W/cm², the temperature difference on the bottom wall is 15.24 ˚C which decreases to 5.15 ˚C when pressure drop is increased to 60 kPa. When heat flux is increased to 1000 W/cm², the temperature difference on the bottom wall increases to 165.51˚C for pressure drop of 10 kPa and 51.14˚C for pressure drop of 60 kPa.

Figure 5 shows the temperature gradient along bottom wall for the combined heat sink with inverse trapezoidal-shaped microchannels respectively when a minimum heat flux of 100 W/cm² and maximum of 1000 W/cm² is applied. The temperature difference for a pressure drop of 10 kPa, heat flux of 100 W/cm² is 16.98˚C and 5.64 ˚C for 60 kPa. These values are 11.4% and 9.5% higher than that of the trapezoidal combined heat sink for pressure drops of 10 kPa and 60 kPa respectively.

Figure 6 shows the temperature gradient along bottom wall for the combined heat sink with hexagonal-shaped microchannels respectively when a minimum heat flux of 100 W/cm^2 and maximum of 1000 W/cm² is applied. The temperature difference for a pressure drop of 10 kPa, heat flux of 100 W/cm² is 16.60 ˚C and 7.25 ˚C for 60 kPa. These values are 8.9% and 7.9% higher than that of the trapezoidal combined heat sink for pressure drops of 10 kPa and 60 kPa respectively.

Table 5 shows a comparison of the thermal performance combined heat sink considered in this study at a high heat flux of 1000 W/cm² based on two criteria, minimized peak temperature and low temperature gradient on the bottom wall.

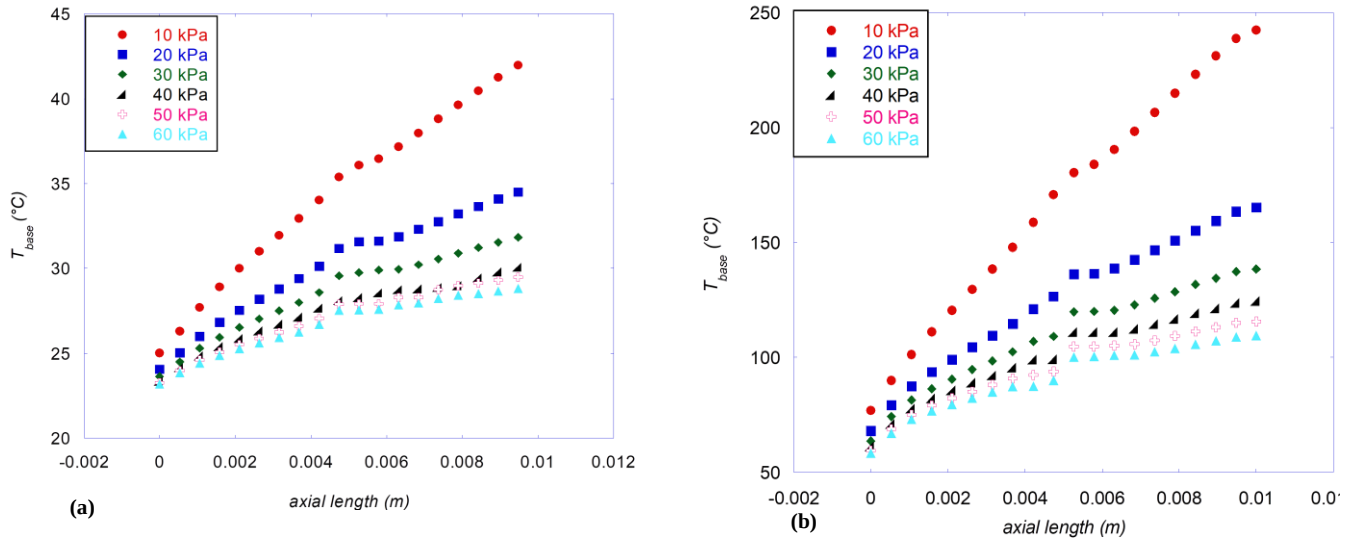

Figure 5: Temperature gradient along the bottom wall of the combined heat sink with inverse trapezoidal-shaped microchannel (a)100 W/cm^2 (b) 1000 W/cm^2.

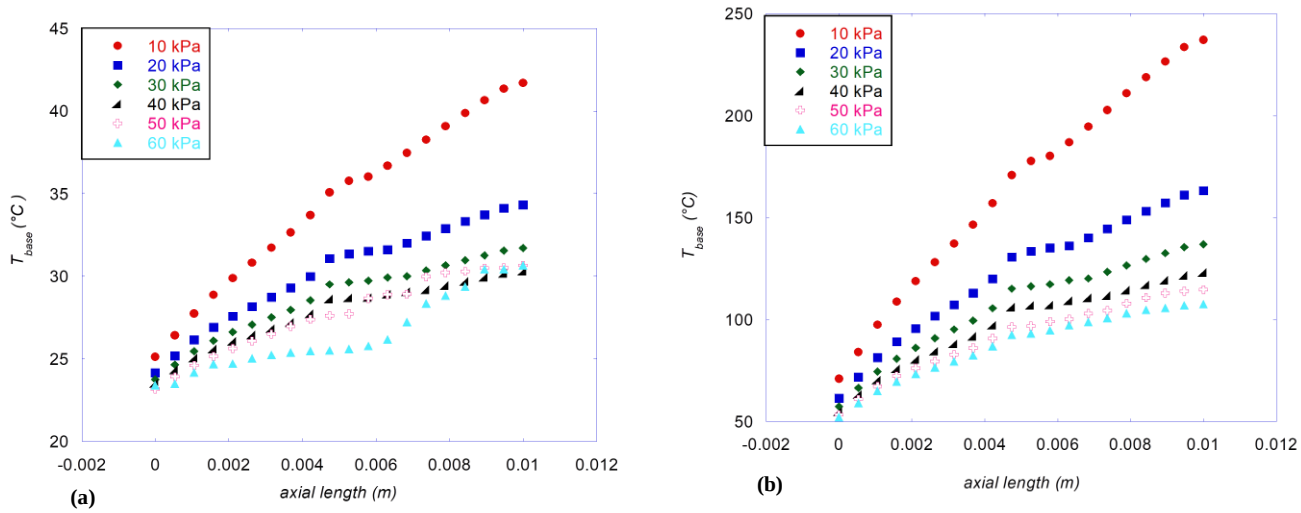

Figure 6: Temperature gradient along the bottom wall of the combined heat sink with hexagonal-shaped microchannel (a)100 W/cm^2 (b) 1000 W/cm^2.

Table 5: Comparison between performances of the combined heat sink based on minimized peak temperature and temperature difference along the bottom wall at heat flux of 1000 W/cm^2

	$(T_{max})_{min}$ °C		$(\Delta T)_{base}$ °C	
Combined Heat Sink	10 kPa	60 kPa	10 kPa	60kPa
Trapezoidal	168.34˚C	91.85˚C	165.50˚C	51.33˚C
Inverse-Trapezoidal	168.45˚C	88.76˚C	173.36˚C	57.13˚C
Hexagonal	165.14˚C	88.03˚C	166.03˚C	55.47˚C

Results presented show at low pressure drops (which relates to pumping power cost), the combined heat sink with hexagonal-shaped microchannel is the chosen option for minimized peak temperature $(T_{max})_{min}$ while the combined heat sink with trapezoidal-shaped microchannel is chosen if minimum thermal gradient on the heated base is the parameter of interest.

V. CONCLUSION

The thermal performance of three separate combined heat sinks with trapezoidal-, inverse trapezoidal, and hexagonal-shaped channels were numerically studied under rising thermal flux. The value of the thermal flux was elevated from $100\ W/cm^2$ to $1000\ W/cm^2$. For a constant pressure drop of 10 kPa and a uniform thermal flux of $1000\ W/cm^2$, the hexagonal combined heat sink exhibited the optimum thermal performance in terms of lowering maximum temperature. The temperature variation results along the heated bottom of the combined heat sink upon investigation showed that the trapezoidal combined heat sink performed well in minimizing the temperature variation along the bottom of the heated substrate.

Due to its thermal performance in maximizing thermal conductance, the hexagonal combined microchannel can be suggested as the ideal heat sink for reducing maximum temperature, while the trapezoidal combined microchannel was the best heat sink for minimizing increasing temperature along the heated base of the combined heatsink under increasing thermal flux.

REFERENCES

Abdel-Rehim, Z. S. (2008). Optimization and thermal performance assessment of pin-fin heat sinks. Energy Sources, Part A: Recovery, Utilization, and Environmental Effects, 31(1): 51-65.

Adewumi, O. O.; T. Bello-Ochende and J. P. Meyer (2013). Constructal design of combined microchannel and micro pin fins for electronic cooling. International Journal of Heat and Mass Transfer, 66: 315-323.

ANSYS FLUENT 14.0 (2011) User's Guide Documentation, ANSYS Inc.

ANSYS FLUENT 14.0 User's Guide, ANSYS, Inc., Southpointe, 2011.

Bello-Ochende, T. (2015). Multi-scale pin fins: Scale analysis and mathematical optimization of micro-pin fins arranged in rows. Open Engineering, 5(1):238-247.

Bello-Ochende, T.; L. Liebenberg and J. P. Meyer. (2007). Constructal cooling channels for micro-channel heat sinks. International Journal of Heat and Mass Transfer, 50(21-22): 4141-4150.

Bello-Ochende, T.; J. P. Meyer and F. U. Ighalo. (2010). Combined numerical optimization and constructal theory for the design of microchannel heat sinks. Numerical Heat Transfer, Part A: Applications, 58(11): 882-899.

Chen, Y.; C. Zhang; M. Shi and J. Wu. (2009). Three-dimensional numerical simulation of heat and fluid flow in noncircular microchannel heat sinks. International Communications in Heat and Mass Transfer, 36(9): 917-920.

Garg, H.; V. S. Negi; A. S. Wadhwa and A. K. Lall. (2014). Numerical analysis of different shapes of microchannel for miniature cooling system. Paper presented at 2014 Recent Advances in Engineering and Computational Sciences (RAECS), Chandigarh, 1-7, India: IEEE.

Glazar, V.; B. Frankovic and A. Trp. (2015). Experimental and numerical study of the compact heat exchanger with different microchannel shapes. International Journal of Refrigeration, 51: 144-153.

Hasan, M. I. and Muter, D. M. (2019). Study the micro pin fin and micro channel heat sinks with different types of cooling fluids. Presented in First International Scientific Conference of Al-Ayen University (ISCAU 2019), Nasiriyah, 0-32, Iraq.

Hasan, M. I. and Tbena, H. L. (2018). Enhancing the cooling performance of micro pin fin heat sink by using the phase change materials with different configurations. Paper presented in 2018 International Conference on Advance of Sustainable Engineering and its Application (ICASEA), Wasit-Kut, 205-209, Iraq: IEEE.

İzci, T.; M. Koz and A. Koşar. (2015). The effect of micro pin-fin shape on thermal and hydraulic performance of micro pin-fin heat sinks. Heat Transfer Engineering, 36(17): 1447-1457.

Jadhav, S. V.; P. M. Pawar and B. P. Ronge. (2018). Analysis of pin-fin geometry effect on microchannel heat sink performance. International Journal of Mechanical and Production Engineering Research and Development, 8(4): 653-666.

Jagadale, V. A.; S. M. Sarange; S. V. Jadhav and A. G. Kamble. (2020). Thermal Analysis of Micro Channel Heat Sink with Various Shapes of Dimples. Techno-Societal 2018: Proceedings of the 2nd International Conference on Advanced Technologies for Societal Applications. Marahashtra, 841-854, India.

Khan, W.A.; A.; J. R. Culham and M. M. Yovanovich. (2006). Performance of shrouded pin-fin heat sinks for electronic cooling. Journal of Thermophysics and Heat Transfer, 20(3): 408-414.

Khan, A. A. and Kim, K. Y. (2013). Performance analysis of various geometrical shapes of microchannel heat sink. Proceedings of the Korean Society of Fluid Mechanics Conference, Jeju, 27-29, South Korea.

Khan, A. A.; S. M. Kim and K. Y. Kim. (2016). Multi-objective optimization of an inverse trapezoidal-shaped microchannel. Heat Transfer Engineering, 37(6): 571-580.

Khan, W. A.; J. R. Culham and M. M. Yovanovich. (2006). The role of fin geometry in heat sink performance. Transactions of the ASME, 128: 324-330.

Magnini, M. and Matar, O. K. (2020). Numerical study of the impact of the channel shape on microchannel boiling heat transfer. International Journal of Heat and Mass Transfer, 150: 119322.

Meyer, J. P.; O. T. Olakoyejo and T. Bello-Ochende. (2012). Constructal optimisation of conjugate triangular cooling channels with internal heat generation. International communications in heat and mass transfer, 39(8): 1093-1100.

Muzychka, Y. S. (2005). Constructal design of forced convection cooled microchannel heat sinks and heat exchangers. Paper presented in International Conference on Nanochannels, Microchannels, and Minichannels, Toronto, Ontario, 647-655, Canada.

Olakoyejo, O. T. and Meyer, J. P. (2014). Numerical optimisation of square pin-fins for minimum thermal resistance with non-uniform design dimensions. International Conference on Heat Transfer, Fluid Mechanics and Thermodynamics (HEFAT 2014), Orlando, Florida, 1244-1251.

Olakoyejo, O. T.; T. Bello-Ochende and J. P. Meyer. (2012). Constructal conjugate cooling channels with internal heat generation. International Journal of Heat and Mass Transfer, 55(15-16): 4385-4396.

Roy, R. and Kundu, B. (2018). Effects of fin shapes on heat transfer in microchannel heat sinks. Heat Transfer—Asian Research, 47(4): 646-659.

Salimpour, M. R.; M. Sharifhasan and E. Shirani. (2013). Constructal optimization of microchannel heat sinks with noncircular cross sections. Heat Transfer Engineering, 34(10): 863-874.

Teja, V. S.; A. Ramakrishna and R. Rao. (2014). Numerical study of different cross-sectional stacked microchannel heat sink. International Journal of Engineering Research & Technology, 3(8): 54-59.

Tuckerman, D. B. and Pease, R. F. W. (1981). High-performance heat sinking for VLSI. IEEE Electron device letters, *2*(5): 126-129.

Wei, X. and Joshi, Y. (2003). Optimization study of stacked micro-channel heat sinks for micro-electronic cooling. IEEE transactions on components and packaging technologies, 26(1): 55-61.

Yadav, S. and Pandey, K. M. (2018). A comparative thermal analysis of pin fins for improved heat transfer in forced convection. Materials Today: Proceedings, 5(1): 1711-1717.